



Characteristics of liquid stannum anode fuel cell operated in battery mode and CO/H₂/carbon fuel mode



Hongjian Wang, Yixiang Shi*, Ningsheng Cai

Key Laboratory for Thermal Science and Power Engineering of Ministry of Education, Department of Thermal Engineering, Tsinghua University, Beijing 100084, China

HIGHLIGHTS

- Smooth electrolyte for inherent reaction characteristics.
- Multi operating modes: battery mode, CO and H₂ gas fuel mode, carbon fuel mode.
- Performance recovery characteristics.

ARTICLE INFO

Article history:

Received 7 March 2013

Received in revised form

20 July 2013

Accepted 24 July 2013

Available online 2 August 2013

Keywords:

Fuel cell

Liquid stannum anode

Smooth electrolyte

Battery mode

Gas fuel

Carbon fuel

ABSTRACT

A liquid Stannum (Sn) anode fuel cell is fabricated by using smooth single crystal Yttria Stabilized Zirconia (YSZ) electrolyte and porous Pt cathode. The cell performance in the battery mode is tested to identify the intrinsic reaction kinetics of the Sn electrochemical oxidation reaction. The cell performance characteristics in the gas fuel mode and carbon fuel mode are experimentally measured to identify limiting steps in different operating modes. The results show that in the battery mode, the SnO₂ film formation blocks the transportation path of the liquid Sn and oxygen ions to the reactive interface. In the gas fuel modes, the cell performance operating in the H₂ fuel mode is much higher than that in the CO fuel mode which is ascribing to the effective reaction of the formed SnO₂ at the reactive interface between electrolyte and anode. In the carbon fuel mode, the carbon black fuel can directly or indirectly reduce part of the SnO₂ at the interface between anode and electrolyte. It apparently indicates that the performance improvements of liquid Sn anode direct carbon fuel cell rely on minimizing the effects of formed SnO₂ layer and accelerating species transportation processes within the liquid Sn electrode.

© 2013 Elsevier B.V. All rights reserved.

1. Introduction

Direct carbon fuel cell (DCFC) is a clean, efficient and competitive power generation technology to convert the chemical energy of solid carbon fuel into electricity [1,2]. Theoretical thermodynamic efficiency of DCFC can even reach 100% as the entropy change of overall reaction C + O₂ = CO₂ is only 2.5 J K⁻¹ mol⁻¹ at 800 °C [3]. Since the carbon fuel and the gas products are distinct phases, the fuel utilization can almost be 100% and the gas product can be easily separated which is beneficial to potential low cost CO₂ capture. In addition, DCFC can be a promising way for the utilization of various solid carbon fuels, such as coal, coke, biomass, waste plastic, etc.

DCFC is still at an early stage of development needing much more efforts in the obstacles related to the cell prototype, materials, reaction kinetics, degradations and system development. One of the innovative types of DCFC is fabricated by solid oxide electrolyte

and liquid metal anode which is usually named liquid metal anode DCFC. In the liquid metal anode DCFC as shown in Fig. 1, the oxygen gas transfers into the porous cathode and is reduced into oxygen ions, which migrate through the electrolyte to the anode. At the liquid metal anode, the liquid metal is oxidized by oxygen ions which result in generation of electrons and then the carbon fuel reduces the metal oxide into metal.

The liquid metal DCFC anode has several special advantages compared with the traditional solid DCFC anode such as Nickel/Yttria Stabilized Zirconia (Ni/YSZ). Firstly, the carbon reaction active area can be effectively increased by changing the contacts between solid electrode and solid carbon fuel into the contact between liquid electrode and solid carbon [4,5]. At the same time, since the liquid metal is electronically conductive, electrochemical reaction can be carried out at the entire interface between the electrolyte and the liquid metal. Secondly, the liquid metal anode itself can be served as the fuel for power generation by the electrochemical reaction between the metal and oxide ions, which can be thought as a kind of energy storage process. And thus the liquid metal anode

* Corresponding author. Tel./fax: +86 10 62789955.

E-mail address: shyx@tsinghua.edu.cn (Y. Shi).

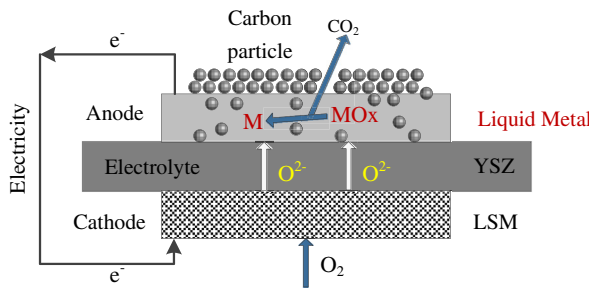


Fig. 1. Basic operating principle of liquid metal anode direct carbon fuel cell.

can be acted as a buffer layer to alleviate the effects of discontinuous fuel supply on DCFC operating stability. The liquid metal anode has relatively higher tolerance in the impurities such as sulfur, NOx which are commonly components in the practical carbon fuel [6]. Also, the ash can float on the surface of liquid metal which can be easily removed.

There are several requirements in choosing appropriate metal for being used as liquid metal anode. The melting temperature of the metal should be below typical SOFC operating temperature (700–900 °C) [7]. At the same time, the metal oxide should be possible to be reduced by the solid carbon fuel spontaneously. The oxidation potential for solid carbon fuel will be near 1 V relative to air, the oxidation potential for spontaneous metal oxidation reaction is less than 1 V [7]. Several types of the liquid metals such as Sn [8–11], Sb [12–14], Ag [15,16], Cu [17] have been examined as the anodes. Ascribing to the low melting point (231 °C) and the high boiling point (2260 °C), Sn has been paid much attention. The low melting point allows for improved oxygen solubility by operating far above its fusion point. The high boiling point provides low vapor pressure (9.87×10^{-4} Pa at 1000 °C [18]) of Sn which is beneficial for long term operation of the cell. Sn also has a high enough OCV at 800 °C (0.897 V), which is roughly 0.1 V lower than the equilibrium value for carbon oxidation to CO₂.

Many efforts have been focused on the liquid metal anode reaction mechanism, effects of impurity in coal and prototype design. CellTech Power LCC firstly used liquid Sn as anode and used coal as fuel to operate for two weeks without fuel processing, reforming or sulfur removal [19]. In order to understand the comprehensive insights of the liquid Sn anode DCFC, the battery mode of liquid Sn anode SOFC in which the liquid Sn acts as the fuel source, the gas fuel mode in which the H₂, CO is used as the fuel, as well as the carbon fuel mode in which the solid carbon is used as the fuel should be studied and compared. When the liquid Sn anode operates in battery mode, it results in formation of metal oxides [10]. During the operation, an insulating SnO₂ layer is formed by electrochemical oxidation of Sn at the electrolyte/metal interface, which limits the Sn-based electrode performance due to the low ionic conductance of this SnO₂ layer. Meanwhile, it should be noted that the roughness have significant effects on the cell performance measurements, especially will lead to the ambiguities and difficulties in the determination of the effective reacting area. Above discussions show the necessities to apply the extremely smooth electrolyte/liquid Sn interface in getting the inherent reaction characteristics between liquid Sn and the oxygen ions, and the detailed comparisons among the liquid Sn anode DCFC performance operated in the battery mode, gas fuel mode and carbon fuel mode.

In the present study, a liquid Sn anode DCFC is fabricated by using smooth single crystal YSZ electrolyte and porous Pt cathode. The cell performance in the battery mode is tested to identify the intrinsic reaction kinetics of the Sn electrochemical oxidation reaction. The polarization curve and electrochemical impedance spectra of the DCFC in different modes are measured. Scanning electron microscopy (SEM) tests are carried out for characterization

of the liquid Sn and electrolyte interface before and after the testing. The cell performances in the gas fuel mode and in the carbon fuel mode are experimentally measured to indentify the limiting steps in different operating conditions.

2. Experiments

2.1. Cell fabrication

A 25 mm diameter single crystal YSZ electrolyte substrate with 13 mol%Y₂O₃ (Crystal orientation <100>, Hefei Kejing Materials Technology Limited Company, China). The roughness of the electrolyte surface Ra is kept at 0.67 nm, and the electrolyte thickness is 500 μ m. The cathode of the cell was prepared from platinum paste (MC-Pt100, Grikin Advanced Materials Limited Company, China) by the screen printing method. The Pt paste layer was dried at 100 °C in air condition for 15 min. The calcination temperature for the cathode composite was set at 800 °C.

After cathode layer preparation, the cell was placed on the end of an alumina tube. An alumina plate was pressed to the button cell to fix it by three springs. There was a sealing glasses ring between the alumina tube and the button cell. On the cathode side, a platinum mesh was used as current collector. On the anode side, a Ni20Cr80 ring was used as the current collector and also used to hold the liquid stannum (Sn) metal electrode above the electrolyte. The alumina tube was then placed to be vertical for keeping the liquid metal in contact with the single crystal YSZ electrolyte. The stannum metal powder and the carbon fuel powder can be added into the anode chamber during the cell operation through the alumina tube in the center. In this study, 2.0 g Sn (99.5%, Sinopharm Chemical Reagent Limited Company, China) is added on top of the electrolyte. The thickness of the liquid metal anode should be around 1.5 mm according to the approximate calculation based on the diameter of the inner diameter of the current collector ring (16 mm) and the density of the liquid Sn at 800 °C (6.6 g cm⁻³ [20]).

2.2. Experimental setup

A direct carbon fuel cell experimental setup has been built for cell performance testing as shown in Fig. 2.

The polarization curves were measured using four-probe method with an electrochemical workstation (IM6ex, Zahner-

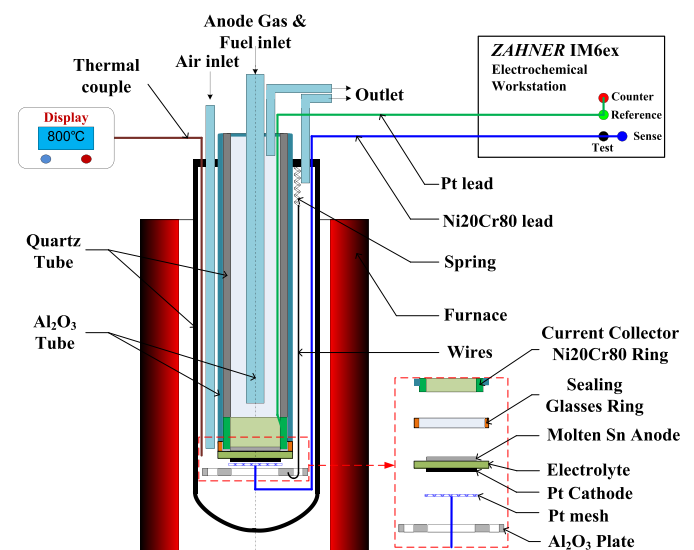


Fig. 2. Liquid Sn anode direct carbon fuel cell experimental testing setup.

Table 1

Testing cases at battery mode, gas fuel mode and carbon fuel mode.

Mode	Temperature	Anode gas	Anode gas flow rate	Cathode gas	Cathode gas flow rate
Battery	800 °C	Ar	50 mL min ⁻¹	Air	200 mL min ⁻¹
Gas fuel	800 °C	H ₂	50 mL min ⁻¹	Air	200 mL min ⁻¹
		CO	50 mL min ⁻¹	Air	200 mL min ⁻¹
Carbon black	800 °C	Ar	50 mL min ⁻¹	Air	200 mL min ⁻¹
		CO ₂	50 mL min ⁻¹	Air	200 mL min ⁻¹

Elektrik GmbH, Germany). Electrochemical impedance spectroscopy (EIS) was performed using amplitude of 20 mV over the frequency from 0.1 Hz to 100 kHz. The ohmic resistance of the cell was estimated from the high frequency intercept of the impedance curve. The measurements were initiated when the system was

stable. A K-type thermal couple was used to test the temperature beside the button cell. The Ar/CO/H₂ mixture gas for the anode chamber and the air for cathode chamber were controlled by mass flow controllers.

During the experimental tests, the button cell was heated up to 800 °C from room temperature by 10 h with Ar shielding gas with flow rate at 35 mL min⁻¹ for both anode and cathode chambers. The platinum paste was sintered for 30 min at 800 °C. The Ar gas flow rate in the anode was then increased to 50 mL min⁻¹, and the cathode gas was switched to air at 200 mL min⁻¹. 2.0 g Sn powder was added into the anode chamber through the alumina tube in the center. During the cell performance testing process, the total flow rate of the anode gas was kept at 50 mL min⁻¹ and the total flow rate of the cathode gas was kept at 200 mL min⁻¹.

The electrochemical characteristics testing cases at different modes are shown in Table 1.

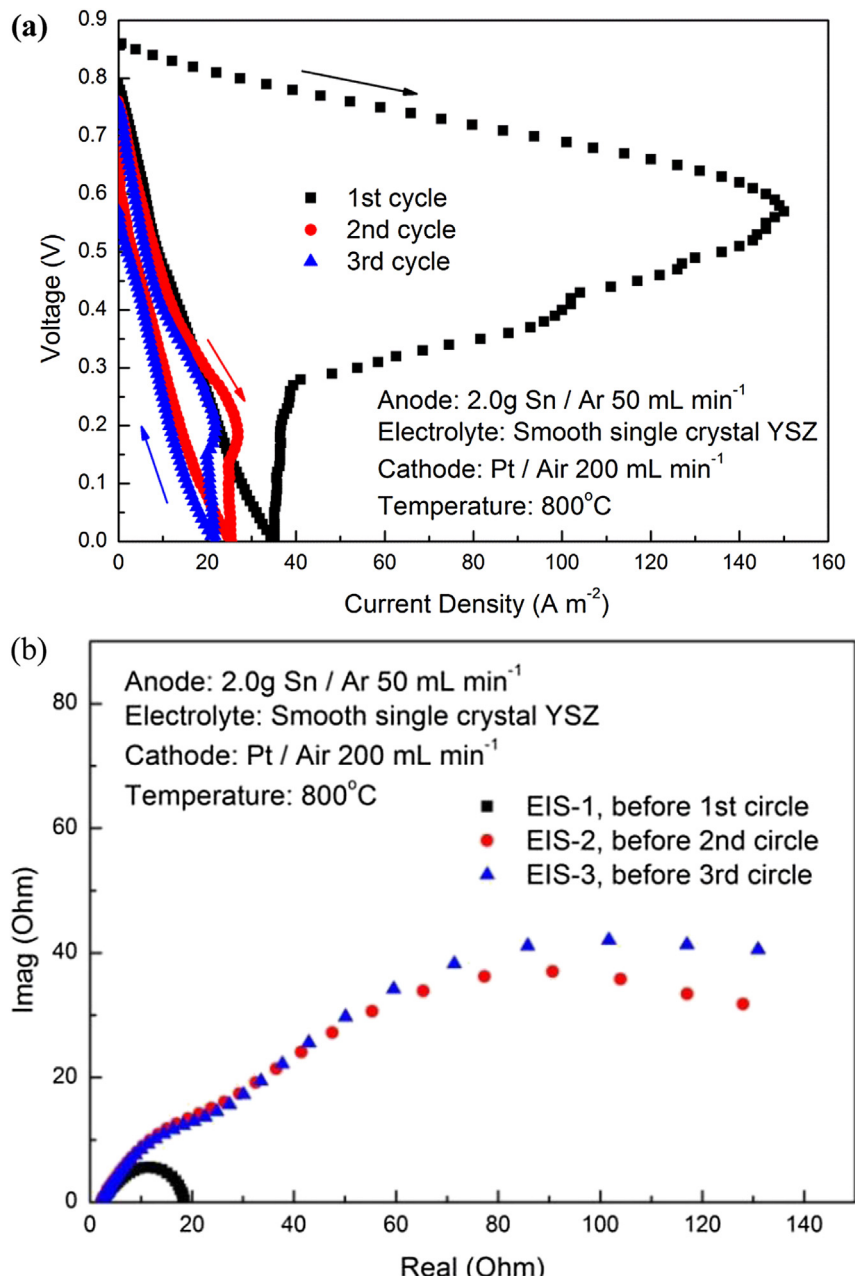


Fig. 3. Liquid Sn anode DCFC performances in the battery mode (a) IV polarization curves (b) EIS spectra.

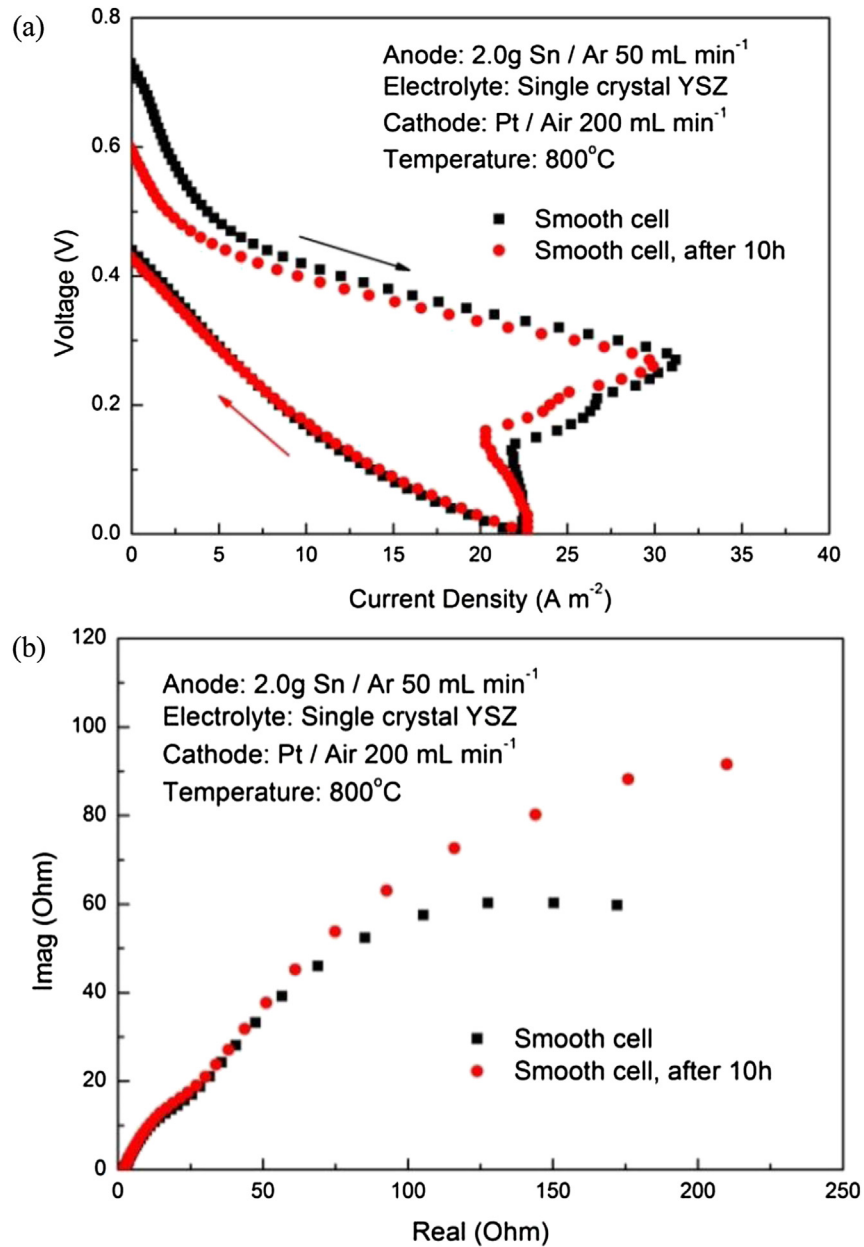


Fig. 4. Liquid Sn anode DCFC performances in the battery mode after and before standing for 10 h (a) IV polarization curves (b) EIS spectra.

3. Results and discussion

3.1. Battery mode

Fig. 3 shows the IV polarization curves and the EIS spectra of the liquid Sn anode fuel cell operating in the battery mode at 1073 K. Before testing at the battery mode, pure hydrogen with the flow rate at 50 mL min^{-1} was set to the anode chamber to reduce the residual oxygen and SnO_2 existed in the liquid Sn. Then the Ar was used as the anode carrier gas. After 1 h operation at open circuit voltage of the Sn anode in the Ar atmosphere, the first IV polarization cycle was tested. After 10 min, the second IV curve was tested, and after another 10 min, the third IV curve was tested. Before testing each IV cycle, the EIS spectra were measured.

The first IV cycle showed that the open circuit voltage (OCV) is 0.862 V which is similar to that theoretical OCV 0.897 V. The shape

of the first cycle curve is obviously different from the second and the third cycle curves. For the first cycle, the forward scanning curve shows that the cell kept relatively higher performance operating between OCV and 0.57 V which is the first turning point, and the current density at this point reached the maximum 150 A m^{-2} . When the cell voltage gets lower than 0.57 V, the current density dramatically decreased from 150 A m^{-2} to 39.4 A m^{-2} where the cell voltage is 0.27 V which is the second turning point. Then, the current density of the cell dramatically decreased to zero with the cell voltage, and the limiting current density in this case was 35.2 A m^{-2} . While, the backward scanning curve shows that the peak value current density was achieved when the cell voltage increased from 0 V to 0.78 V. This transient characteristic shows that the SnO_2 formed by Sn electrochemical oxidation quickly covered the electrolyte/liquid Sn reactive interface and deteriorated the cell performance. The OCV of the following two IV cycles are kept relatively

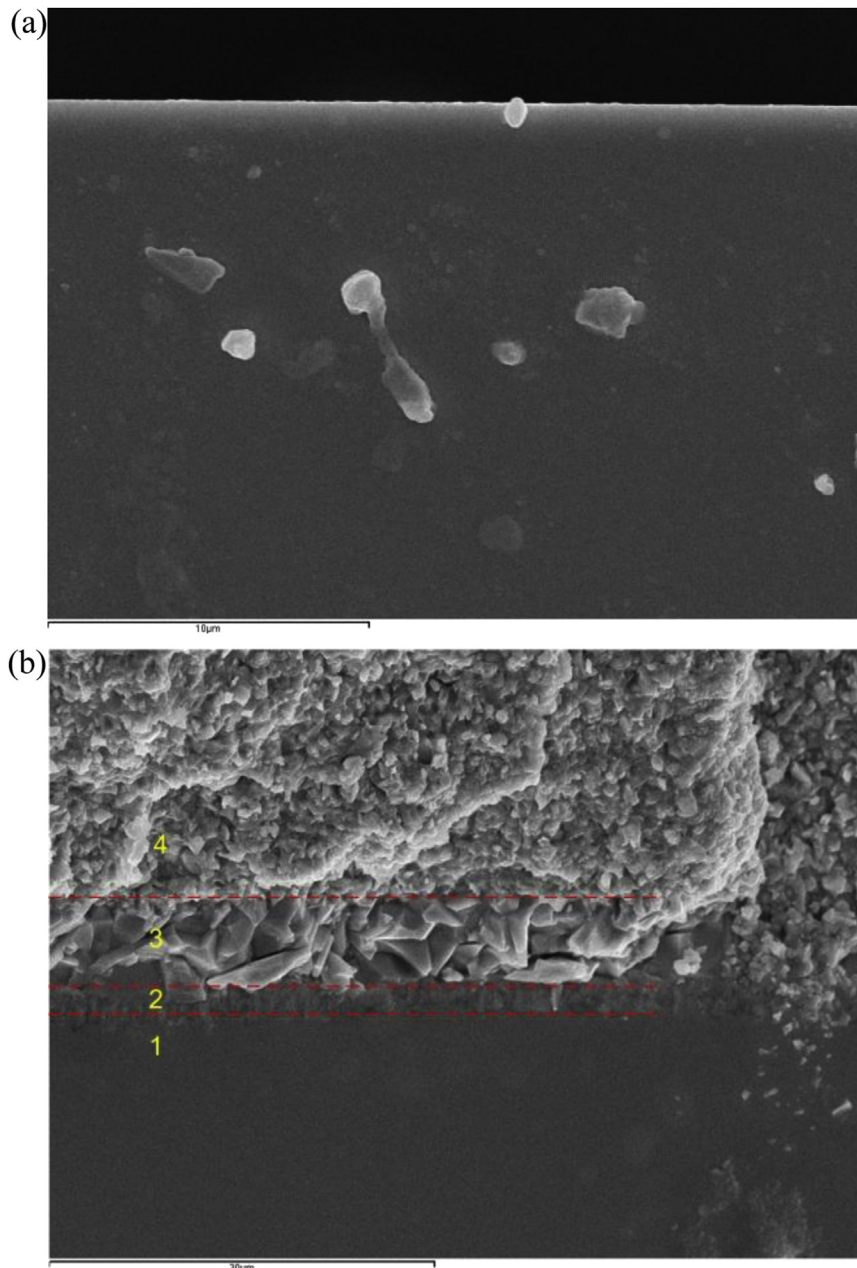


Fig. 5. SEM images of electrolyte crossing section in the battery mode (a) before testing (b) after testing.

steady at 0.75 V. The similar two turning points are shown in these two curves as in the first scanning curve. The first turning points for forward scanning curves are 0.19 V and 0.2 V in the second and the third cycles. The maximum current densities in the two cycles are 26.92 A m^{-2} and 21.82 A m^{-2} . The second turning points for forward

scanning curves are 0.14 V and 0.15 V in the second cycle and the third cycle. While the limiting current densities decreased to 25.4 A m^{-2} and 21.7 A m^{-2} separately, the backward scanning curves for the second cycle and the third cycle were almost straight lines with the decreasing OCV at 0.68 V and 0.56 V.

It can be also predicted by EIS spectra in Fig. 3(b) that during different cycles, the cell ohmic resistance is kept almost the same around 2.3Ω . The changes of the impedance are mainly due to the non-ohmic losses which can be determined from the length of the arc under the Nyquist plot of the EIS spectra. And the cathode polarization should be also the same since there are no changes in the cathode operating. While, it can be seen that the anodic polarization loss increased dramatically after the first cycling operating of liquid Sn anode. This phenomenon further demonstrates the possibilities of forming a SnO_2 film on the electrolyte surface.

Table 2

Chemical element molar percentage in each layer of button cell section by EDS.

Layer name	Chemical element molar percentage (%)			
	Sn	Y	Zr	O
Layer 1	0	7.89	31.86	60.24
Layer 2	7.50	0	32.72	59.78
Layer 3	38.78	0	0	61.22
Layer 4	32.18	0	0	67.82

And the cell performance quickly decreased since it was difficult to detach the formed SnO_2 film apart from the electrolyte reactive surface.

Further, the cell was kept at standing state for 10 h, and then the IV curves and EIS spectra were tested as shown in Fig. 4(a) and (b). The results indicate that the cell performance can not be improved when OCV decrease from around 0.7 V–0.6 V. It can be further deduced that the performance deterioration due to formed SnO_2 film can hardly be improved by SnO_2 diffusion process.

After above cycling testing, SEM images were used to observe the cross section as shown in Fig. 5(b). And the SEM images of the electrolyte cross section before testing is shown in Fig. 5(a) for comparison. The SEM images shows that there were clearly three layers on top of the electrolyte substrate. Based on the analysis on Energy-dispersive X-ray spectroscopy (EDS) testing results as shown in Table 2, it can be deduced that the three layers are

porous SnO_2 , crystal SnO_2 (thickness around 8 μm), SnSZ (thickness around 2.4 μm) from top to bottom. And the formation of the SnSZ shows that the liquid Sn can merge into the surface of the single crystal YSZ surface and react with YSZ to form the dense oxide film.

3.2. Gas fuel mode: H_2 and CO

In order to study the gas fuel transportation and chemical reaction, firstly discharge the cell in the battery mode at 800 °C until the cell OCV was lower than 0.6 V and limit current density was lower than 10 A m^{-2} as shown in Fig. 5(a). Then switch gas into 50 mL min^{-1} H_2 or 50 mL min^{-1} CO .

Fig. 6 shows the IV polarization curves and the EIS spectra at H_2 fuel mode, CO fuel mode and battery mode. By comparing the cell performance curves in the H_2 fuel mode with that in the battery

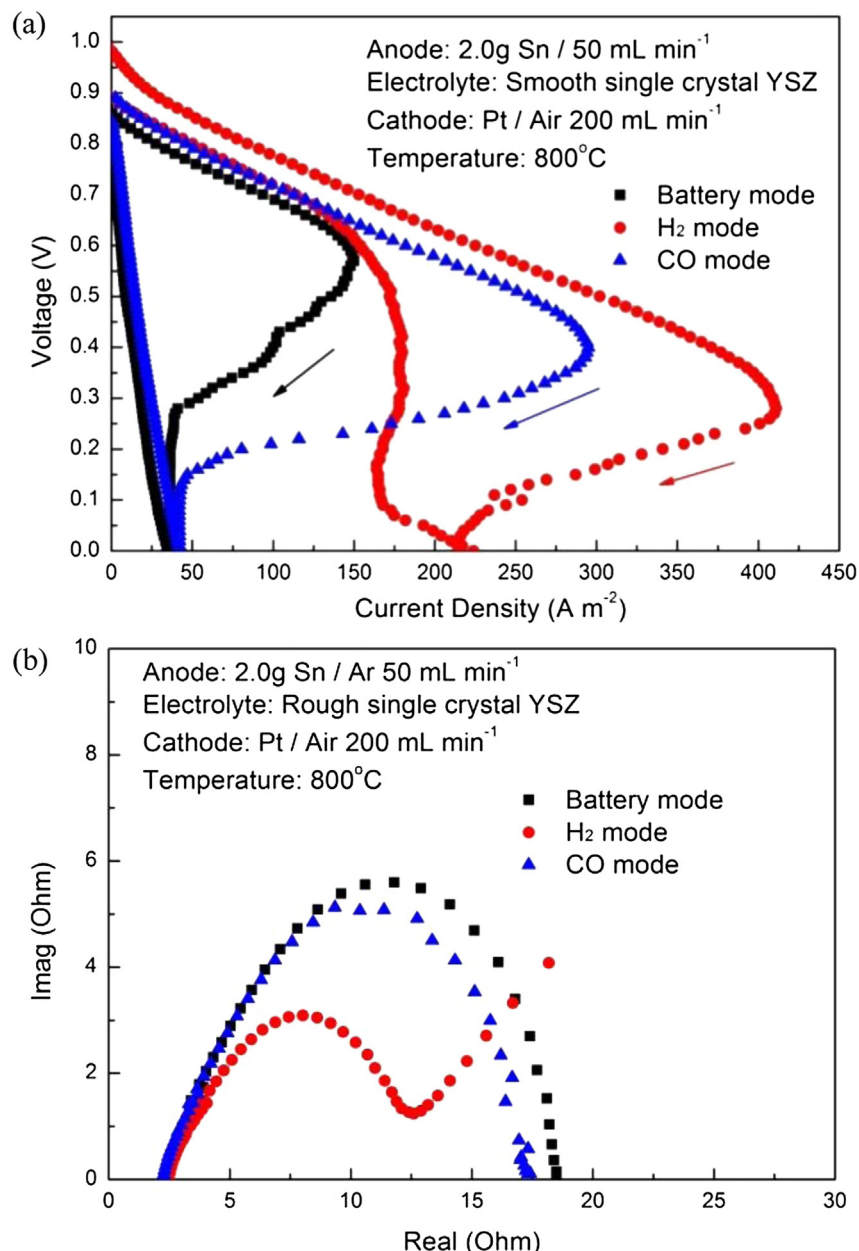


Fig. 6. Liquid Sn anode DCFC performances in the gas fuel mode (a) IV polarization curves (b) EIS spectra.

mode, it can be seen that the OCV in the H_2 fuel mode can reach up to 0.99 V which is much higher than that in the battery mode 0.86 V. This is mainly because that dissolved hydrogen species can transport to the electrolyte/liquid Sn anode interface and oxygen partial pressure at the interface is controlled both by the hydrogen and the liquid Sn. The limiting current density of the cell at the H_2 fuel mode is almost four times as that of battery mode which is still ascribing to the hydrogen transportation from fuel gas bulk to the electrolyte/liquid Sn interface and hydrogen participation in the electrochemical reactions. However, when the cell voltage decreased to 0.25 V, there was a performance turning point due to the accumulation of SnO_2 products. It should be noted that the backward scanning curve is still lower than the forward scanning curve which indicates that the hydrogen diffusion rate in liquid Sn anode is still slower than the hydrogen consumption rate in this condition.

When the cell is operated in the CO fuel mode, the OCV is kept at around 0.89 V which is a little bit higher than the OCV when the cell is operated in the battery mode 0.86 V, and is lower than the OCV when the cell is operated in the H_2 fuel mode. It indicates that CO can transport to the interface but the CO at the electrolyte/liquid Sn anode interface is not adequate. In this situation, the cell OCV is governed by both of the Sn and CO electrochemical oxidation reactions. At the same time, since the CO partial pressure at the electrolyte/liquid Sn interface is relatively low, only part of SnO_2 at the electrolyte surface could be reduced. Different from the cell performance in the battery mode, the cell performance turning point in the CO fuel mode is at around 0.4 V which is lower than in the battery mode 0.57 V. It indicates that the CO can transport to the electrolyte/liquid Sn anode interface and can depress the formation of SnO_2 layer. However, it can be seen that the limiting current density in the CO fuel mode 42 A m^{-2} was close to the

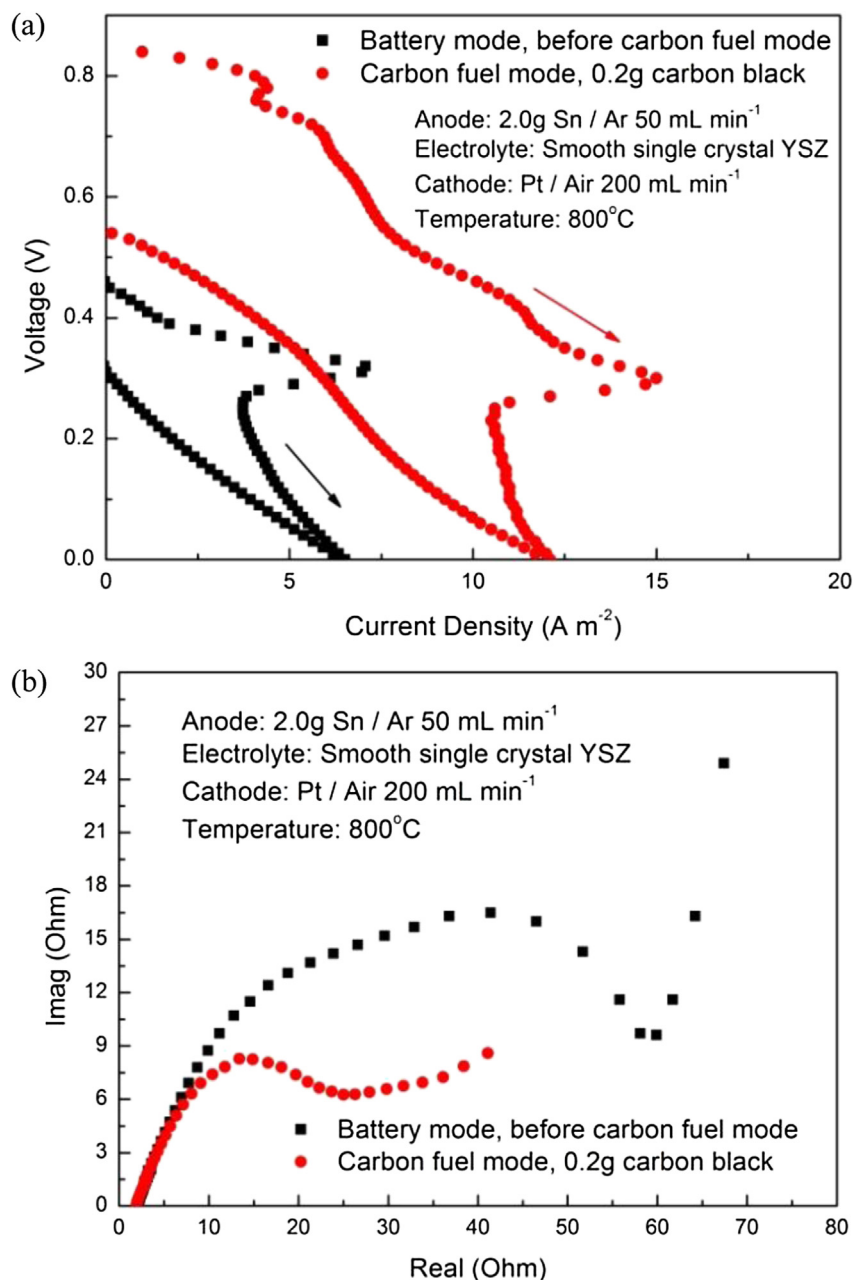


Fig. 7. Performance comparisons of liquid Sn anode DCFC in the battery mode and carbon fuel mode (a) IV polarization curves (b) EIS spectra.

limiting current density in the battery mode 35 A m^{-2} , which indicates that CO transportation process within liquid Sn anode is rather slow and it is difficult to quickly reduce the SnO_2 film produced by electrochemical oxidation reactions. And also, it further demonstrates that CO diffusion rate in the liquid Sn bulk is much lower than that of H_2 so that only part of formed SnO_2 in the battery mode is reduced and the performance decreases. The backward scanning curve was lower than forward scanning curve which further shows that the formed SnO_2 layer is difficult to be reduced.

From the EIS spectra in Fig. 6(b), it can be seen that the ohmic contribution to the impedance, around 2.3Ω is unchanged in three operating modes. And at the low frequency part in the EIS spectra in the H_2 fuel mode apparently shows the straight lines due to Warburg diffusion impedance, which is a characteristic of a diffusion process. The shapes of the arcs of the EIS spectra in the CO fuel mode and the battery mode are almost same with the non-ohmic losses in the CO fuel mode is a little bit smaller than that in the battery mode. It can be further deduced that the CO is able to reduce partial formed SnO_2 layer but hardly to get good performance as that in the H_2 fuel mode due to difficulties for CO transportation to reactive interface in the liquid Sn anode.

3.3. Carbon fuel mode

Fig. 7(a) shows the IV polarization curves of liquid Sn anode DCFC operating in the carbon fuel mode fueling with carbon black with the anode carrier gas Ar at 50 mL min^{-1} Ar. Before the carbon fuel mode testing, the cell discharged in the battery mode until the cell OCV was lower than 0.6 V and the limit current density was lower than 10 A m^{-2} as shown in Fig. 7. Then, 0.2 g black carbon was added in the anode chamber and cell performance was tested. After 45 min, another IV curve was tested. It can be seen that the cell OCV increased to 0.7 V from 0.6 V after adding the black carbon and remained stable. It suggests that the carbon black fuel can effectively depress the oxygen partial pressure in the liquid Sn anode. While, the cell performance only increased a little bit with almost the same limiting current density at around 12.5 A m^{-2} . The backward scanning IV curve of the cell in the carbon fuel mode was almost the same with that in the battery mode. The experimental results suggest that it is quite difficult for carbon fuel to have impacts on the reactive interface between liquid anode and electrolyte. The cell performance is still governed mainly by the liquid Sn electrochemical oxidation processes. The EIS spectra in Fig. 7(b) shows that the ohmic resistance and the cathode polarization loss were almost unchanged, while the concentration polarization loss decreased. It further illustrates that the carbon fuel is difficult to transport to the interface between anode and electrolyte.

Fig. 8 shows the performance of liquid Sn anode DCFC in the carbon fuel mode with the interval time between the curves for more than 10 h. Comparing with Fig. 7, it can be seen that the OCV recovered from 0.55 V to 0.75 V after 10 h, while this value was still smaller than the initial state of 0.85 V . While, the cell limiting current density after standing for 10 h improved from 12 A m^{-2} to 30 A m^{-2} . It demonstrates that the carbon black fuel can have the positive impacts on cell performance, especially can reduce part of the formed SnO_2 after a relatively longer interval. However, since the carbon diffusion rate in the liquid Sn anode is much slower than that of the gas species, the SnO_2 is probably mainly be reduced by the gas product, such as CO from solid carbon reaction with SnO_2 or CO_2 . And, it also can be found a sudden drop in the forward scanning polarization curve. It apparently shows the effect of produced CO on the cell performance is the same characteristics of the cell performance curve in the CO gas fuel mode. It illustrates that the carbon fuel can directly or indirectly reduce part of the SnO_2 at the interface between anode and electrolyte, however, the concentration

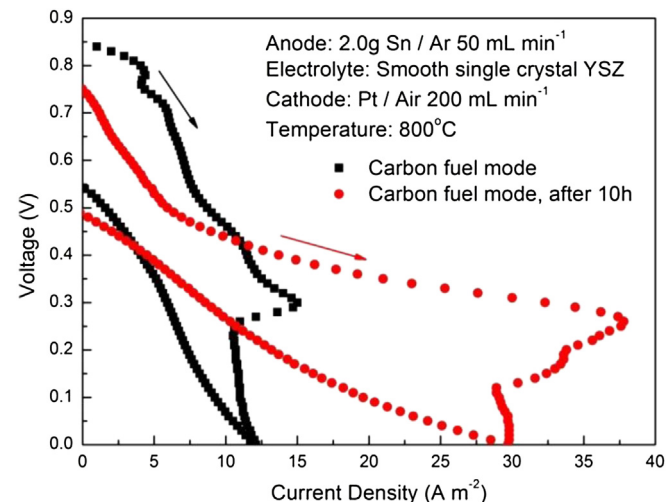


Fig. 8. IV polarization curves for liquid Sn anode DCFC in the carbon fuel mode.

polarization loss due to the accumulation of the produced SnO_2 layer is still one of the main resistances affecting the cell performance. It apparently indicates that the performance improvements with liquid Sn anode DCFC require minimizing the losses due to the formed SnO_2 , for example, by accelerating the effective fuel species transport processes within the liquid Sn electrode.

4. Conclusions

A liquid Sn anode DCFC is fabricated by using smooth single crystal YSZ electrolyte and porous Pt cathode. The cell performance in the battery mode is tested to identify the intrinsic reaction kinetics of the Sn electrochemical oxidation reaction. Experimental results indicate that in the battery mode, the SnO_2 film formation blocks the transportation path of the liquid Sn and oxygen ions to the reactive interface. Since the formed SnO_2 is porous, the oxygen partial pressure at the electrolyte/liquid Sn anode interface increases. The concentration polarization loss increases quickly with the accumulation of SnO_2 product layer during cell operation.

When the liquid Sn anode DCFC is operated in the gas fuel modes, H_2 can effectively reduce the formed SnO_2 at the reactive interface between electrolyte and anode, and greatly improves the cell performance. Since CO diffusion rate in the liquid Sn is much slower than that of H_2 so that only part of formed SnO_2 in the battery mode is reduced and the performance decreases. When the cell is operated in the carbon fuel mode, it is difficult for carbon fuel to have impacts on the reactive interface between liquid anode and electrolyte. The cell performance is still governed mainly by the liquid Sn electrochemical oxidation processes. The cell performance improvement after standing for more than 10 h demonstrates that the carbon black fuel can directly or indirectly reduce part of the SnO_2 at the interface between anode and electrolyte; however, the concentration polarization loss due to the accumulation of the produced SnO_2 layer is still one of the main resistances affecting the cell performance. It apparently indicates that the performance improvements with liquid Sn anode DCFC rely on minimizing the losses due to the formed SnO_2 and accelerating the effective fuel species transport processes within the liquid Sn electrode by fluidizing bed electrode or stirring.

Acknowledgments

This work was supported by the National Natural Science Foundation of China (20776078, 51106085) and the Seed Funding of Low Carbon Energy University Alliance.

References

- [1] D.X. Cao, Y. Sun, G.L. Wang, *J. Power Sources* 167 (2007) 250–257.
- [2] R.H. Wolk, S.M. Lux, S. Gelber, F.H. Holcomb, ERDC-CERL Fuel Cell Program Report, 2007.
- [3] S. Giddey, S.P.S. Badwal, A. Kulkarni, C. Munnings, *Prog. Energ. Combust.* 38 (2012) 360–399.
- [4] T. Tao, in: Proceedings of the 9th International Symposium Solid Oxide Fuel Cells, vol. 1, 2005, pp. 353–362.
- [5] T.M. Gur, *J. Electrochem. Soc.* 157 (2010) B751–B759.
- [6] T.T. Tao, W. McPhee, M. Koslowske, J. Bentley, M. Slaney, L. Bateman, *ECS Trans.* 25 (2009) 1115–1124.
- [7] A. Javadekar, A. Jayakumar, R.J. Gorte, J.M. Vohs, D.J. Buttrey, *J. Electrochem. Soc.* 158 (2011) B1472–B1478.
- [8] M. LaBarbera, M. Fedkin, S. Lvov, *ECS Trans.* 35 (2011) 2725–2734.
- [9] W.A.G. McPhee, L. Bateman, M. Koslowske, M. Slaney, Z. Uzep, J. Bentley, T. Tao, *J. Fuel Cell Sci. Tech.* 8 (2011) 041007-1–041007-5.
- [10] A. Jayakumar, S. Lee, A. Hornés, J.M. Vohs, R.J. Gorte, *J. Electrochem. Soc.* 157 (2010) B365–B369.
- [11] R. Gemmen, H. Abernathy, K. Gerdes, M. Koslowske, W.A. McPhee, T. Tao, *Amer. Ceramic Soc.* 5 (2010) 37–52.
- [12] A. Jayakumar, R. Küngas, S. Roy, A. Javadekar, D.J. Buttrey, J.M. Vohs, R.J. Gorte, *Energ. Environ. Sci.* 4 (2011) 4133–4137.
- [13] A. Jayakumar, J.M. Vohs, R.J. Gorte, *Ind. Eng. Chem. Res.* 49 (2010) 10237–10241.
- [14] A. Javadekar, A. Jayakumar, R.J. Gorte, J.M. Vohs, D.J. Buttrey, *J. Electrochem. Soc.* 159 (2012) A386–A389.
- [15] A. Javadekar, A. Jayakumar, R. Pujara, J.M. Vohs, R.J. Gorte, *J. Power Sources* 214 (2012) 239–243.
- [16] S. Pati, K.J. Yoon, S. Gopalan, U.B. Pal, *J. Electrochem. Soc.* 156 (2009) B1067–B1077.
- [17] K.T. Jacob, *ECS Trans.* 35 (2011) 573–582.
- [18] J.M. Bentley, in: Fuel Cell Seminar, San Antonio, Texas, 2010.
- [19] T. Tao, in: Direct Carbon Fuel Cell Workshop, Pittsburgh, PA, 2003.
- [20] L.W. Wang, Q.S. Mei, *J. Mater. Sci. Technol.* 22 (2006) 569–571.